

# Dynamic phenotypes as criteria for model discrimination: fold-change detection in *R. sphaeroides* chemotaxis

Abdullah Hamadeh, Brian Ingalls, Eduardo Sontag

## Abstract

The chemotaxis pathway of the bacterium *Rhodobacter sphaeroides* has many similarities to the well-studied pathway in *Escherichia coli*. It exhibits robust adaptation and has several homologues of the latter's chemotaxis proteins. Recent theoretical results have been able to correctly predict that the chemotactic response of *Escherichia coli* exhibits the same output behavior in response to scaled ligand inputs, a dynamic property known as fold-change detection (FCD), or input-scale invariance. In this paper, we present theoretical assumptions on the *R. sphaeroides* chemotaxis sensing dynamics that can be analytically shown to yield FCD behavior in a specific ligand concentration range. Based on these assumptions, we construct two models of the full chemotaxis pathway that are able to reproduce experimental time-series data from earlier studies. To test the validity of our assumptions, we propose a series of experiments in which our models predict robust FCD behavior where earlier models do not. In this way, we illustrate how a dynamic phenotype such as FCD can be used for the purposes of discriminating between two models that reproduce the same experimental time-series data.

## 1 Introduction

Dynamic models of biological mechanisms are meaningful if they can explain experimental data, make *a priori* predictions of biological behavior and be liable to invalidation through testing.

Although several competing models of a given mechanism can often be made to reproduce experimental data through sufficient parameterization and tuning, in many cases it is possible to discriminate between such models by comparing the experimentally observed output response and the simulated response to a judiciously designed perturbation. This paper is a study of the use of a particular *dynamic phenotype* for the purposes of model discrimination. Dynamic phenotypes are distinctive, qualitative, dynamic output responses that are robustly maintained under a range of experimental conditions.

An example of a dynamic phenotype is adaptation, where a system initially at steady-state reacts to input stimuli and then restores its pre-stimulus equilibrium. It has been shown that integral control is the structural feature responsible for this behavior [15]. Weber's law, whereby a system exhibits the same maximal amplitude in its response to two different inputs that are positive linear scalings of each other [5] is another example of a dynamic phenotype.

This paper deals with a third dynamic phenotype, termed fold change detection (FCD) [5], or scale invariance. A system is said to exhibit FCD if its output responses to two

different input stimuli that are positive linear scalings of each other are identical (which makes this a stronger property than Weber’s law).

In a study [5, 1], it was predicted that the chemotaxis system of *Escherichia coli*, modeled in [10], would exhibit the FCD property, and these predictions were later confirmed as accurate [2]. The key assumption of this model, which leads to FCD, is the allosteric signaling structure of the methyl-accepting chemotaxis protein receptors.

Although significantly more complex, the chemotaxis system of the bacterium *Rhodobacter sphaeroides* has many similarities to that of *E. coli*. It features two, rather than one, sensory clusters; one at the cell membrane and the other in the cytoplasm. Whilst the membrane cluster, as in *E. coli*, detects external ligand, it is as yet unknown exactly what the cytoplasmic cluster senses [3]. Besides detecting internalized ligand concentrations, it may also sense internal signals, such as signals reporting the cell’s metabolic state. This bacterium also has multiple homologues of the *E. coli* chemotaxis proteins, which play roles similar to those found in the latter, although the exact structure of their connectivity with the two sensory clusters and the flagellum is not known with certainty. The CheA homologues transduce the receptor activity to the other chemotaxis proteins through phosphotransfer, the CheR and CheB homologues respectively methylate and demethylate receptors, whilst the CheY proteins are believed to have a role in varying the stopping frequency of the bacterium’s single flagellum [9].

Recent studies have used a model invalidation technique to suggest possible connectivities for the CheY proteins [8] and the CheB proteins [4]. However, upon simulation it becomes evident that these models do not exhibit the FCD behavior observed in *E. coli*. This suggests the question: given the similarities between the two chemotaxis pathways, does the *R. sphaeroides* chemotaxis response show FCD as does that of *E. coli*?

In this paper, we model the dynamics of the two *R. sphaeroides* receptor clusters using the MWC allosteric model [17] that has been used to model the receptor activity in *E. coli* in [13, 12, 10]. We present a theorem that shows that if this is an accurate model of the receptor dynamics, then the receptor activities will exhibit FCD. What is more, this observed behavior is robust to the connectivity between the chemotaxis proteins, the receptors and the flagellum. To illustrate this point, we construct two models of the integrated *R. sphaeroides* chemotaxis pathway based on our receptor dynamics assumptions, with each model featuring a different connectivity. We show that, in addition to reproducing previously published experimental data, these models also display FCD in their flagellar responses in certain ligand concentration ranges. Since flagellar outputs can be easily measured using tethered cell assays, we then suggest a series of experiments that can be used to test whether the models we present here are accurate compared to previously published models based on whether or not the flagellar response exhibits FCD.

This work therefore makes the case that qualitative dynamic behavior could be a powerful property to test when discriminating between competing models. A systematic way of model discrimination using this approach would start with the construction of a dynamic model that explains experimental data. The next step would be to use the model to mathematically identify experimentally implementable conditions under which the system can be expected to exhibit a certain dynamic phenotype. The final step would be to experimentally implement those conditions and to compare the measured results against what is predicted *in silico*. In this way, two models which explain experimental data equally well can be discriminated using their dynamic phenotypes.

## 1.1 Background

We can decompose the *R. sphaeroides* chemotaxis pathway into three modules, as illustrated in Figure 1. The sensing module includes two receptor clusters. One of these resides at the cell membrane and senses the concentration of external ligands  $L$ , as illustrated in Figure 2. The other cluster resides within the cytoplasm and measures an internalized ligand concentration  $\tilde{L}$ . Henceforth, the  $\tilde{\cdot}$  notation will be used to denote signals associated with the cytoplasmic cluster.

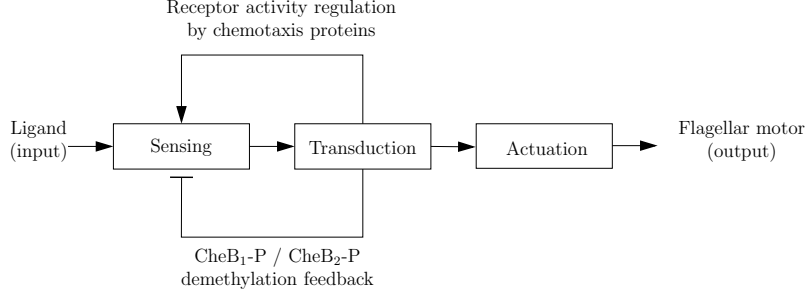


Figure 1: Schematic of the *R. sphaeroides* chemotaxis pathway.

The dynamics of the two receptor clusters are modeled as two first-order systems. The membrane receptor cluster is assumed to have state  $m$  (its receptor methylation level) and output  $a$  (the receptor activity level). Similarly the cytoplasmic cluster has methylation level  $\tilde{m}$  as its state and its activity level  $\tilde{a}$  as its output. The state-space representation of this system is then

$$\begin{aligned}
 \dot{m} &= F(a, w) \\
 a &= G(m, L) \\
 \dot{\tilde{m}} &= \tilde{F}(\tilde{a}, \tilde{w}) \\
 \tilde{a} &= \tilde{G}(\tilde{m}, \tilde{L})
 \end{aligned} \tag{1}$$

where  $w, \tilde{w}$  are functions of the concentrations of the phosphorylated chemotaxis proteins within the cell. These functions represent the interactions between the internal state of the cell and the receptors. For example,  $w$  and  $\tilde{w}$  can represent the demethylation of the receptors by the proteins CheB<sub>1</sub>, CheB<sub>2</sub> or their methylation by the proteins CheR<sub>2</sub>, CheR<sub>3</sub>.

The cytoplasmic cluster is believed to integrate the extra-cellular ligand concentration  $L$  with internal cell signals. We represent these internal cell signals by  $u$ , a function of the concentrations of the phosphorylated chemotaxis proteins. The signal  $\tilde{L}$  in Figure 2 is assumed to have the following relation with the externally sensed ligand.

**Assumption 1.** *The internalized ligand concentration  $\tilde{L}$  is related to the external ligand concentration  $L$  through a linear, time invariant filter*

$$\begin{aligned}
 \dot{\xi} &= A\xi + B(u)L^\nu, \quad \xi \in \mathbb{R}^n \\
 \tilde{L} &= C\xi + D(u)L^\nu
 \end{aligned}$$

where  $A \in \mathbb{R}^{n \times n}$ ,  $B : \mathbb{R} \rightarrow \mathbb{R}^n$ ,  $C \in \mathbb{R}^{1 \times n}$ ,  $D : \mathbb{R} \rightarrow \mathbb{R}$  and  $\nu \in \mathbb{R}$ .

With Assumption 1, the internalized ligand concentration  $\tilde{L}$  can represent a variety of signals, including, for example, a static map that combines the externally sensed ligands  $L$

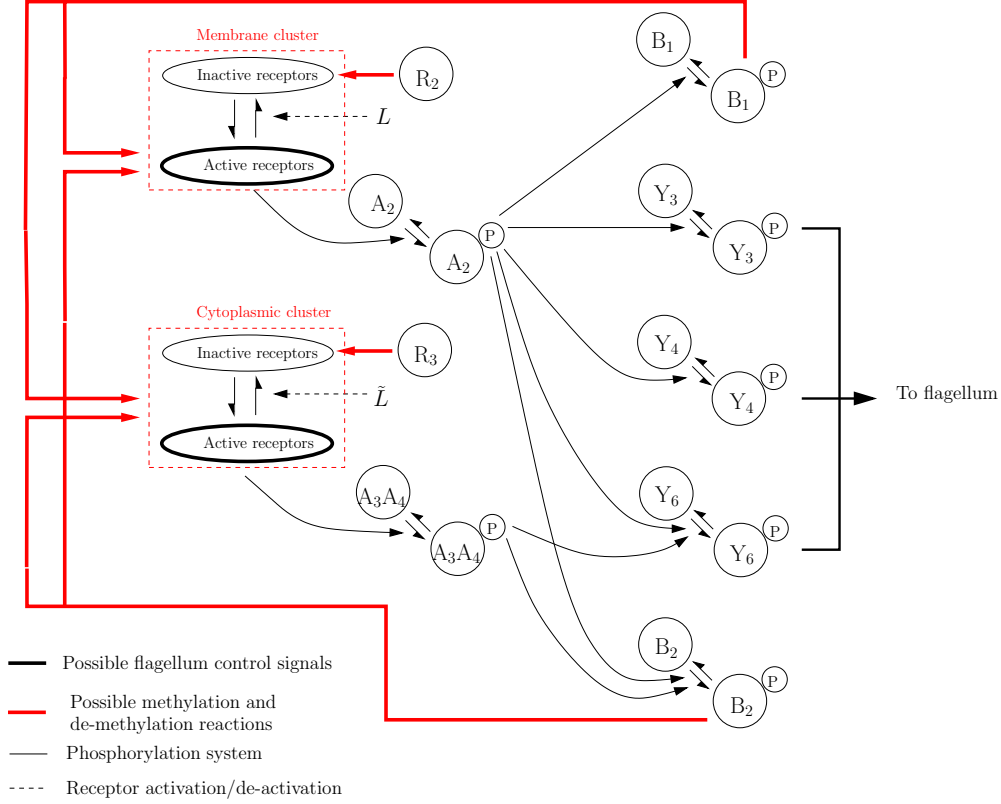


Figure 2: The *R. sphaeroides* signalling network.

with the internal chemotaxis protein signals  $u$ , or it can be a phase-delayed version of  $L$  or even, to allow for a degree of possible cooperativity, a power of  $L$ .

In the transduction sub-system of Figure 1, auto-phosphorylation of the chemotaxis protein CheA<sub>2</sub> is accelerated by the membrane cluster activity, whilst that of the CheA<sub>3</sub>A<sub>4</sub> complex is catalyzed by cytoplasmic cluster activity (as shown in Figure 2). The proteins CheY<sub>3</sub>, CheY<sub>4</sub>, CheY<sub>6</sub>, CheB<sub>1</sub> and CheB<sub>2</sub> all compete for phosphoryl groups from CheA<sub>2</sub>, whilst CheB<sub>2</sub> and CheY<sub>6</sub> do so from CheA<sub>3</sub>A<sub>4</sub>. The reaction rates for all of these phosphorylations are given in [14, 8]. We represent this phosphotransfer network as a general nonlinear system, with state vector

$$\mathbf{x} = [A_{2_p} \ Y_{3_p} \ Y_{4_p} \ (A_3A_4)_p \ Y_{6_p} \ B_{1_p} \ B_{2_p}]^T$$

the individual states being the concentrations of the phosphorylated chemotaxis proteins. The transduction system takes as its inputs the receptor activities  $a, \tilde{a}$ :

$$\dot{\mathbf{x}} = H(\mathbf{x}, a, \tilde{a}) \quad (2)$$

where  $H(\mathbf{x}, a, \tilde{a})$  is given by the ODEs (9)-(15) in [8].

The outputs of this system are signals  $w(\mathbf{x}), \tilde{w}(\mathbf{x}), u(\mathbf{x}, a)$ , which feed back into the sensing subsystem, as described above. The interconnection of the phosphotransfer network

(2) with the receptor dynamics is illustrated in Figure 3, and the interconnection between the two subsystems can thus be written as

$$\begin{aligned}
\dot{m} &= F(a, w(\mathbf{x})), \quad a = G(m, L) \\
\dot{\tilde{m}} &= \tilde{F}(\tilde{a}, \tilde{w}(\mathbf{x})), \quad \tilde{a} = \tilde{G}(\tilde{m}, \tilde{L}) \\
\dot{\xi} &= A\xi + B(u(\mathbf{x}, a))L^\nu, \quad \tilde{L} = C\xi + D(u)L^\nu \\
\dot{\mathbf{x}} &= H(\mathbf{x}, a, \tilde{a})
\end{aligned} \tag{3}$$

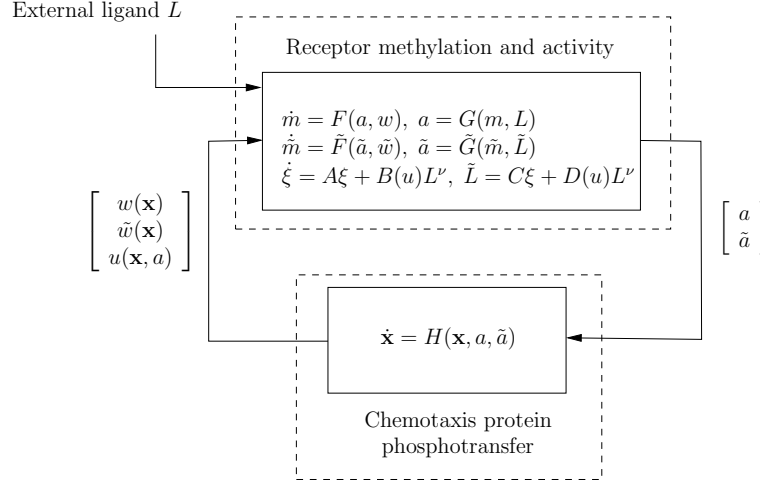


Figure 3: The interconnection of the receptors' sensing dynamics with the phosphotransfer network.

As shown in Figure 2, the protein CheY<sub>6</sub>-P, possibly acting together with one or both of CheY<sub>3</sub>-P and CheY<sub>4</sub>-P, is believed to bind with the flagellar motor proteins to inhibit the flagellar rotation rate [9] (thus effectively coupling the signal transduction system to the actuation system), though the precise mechanism through which this is achieved is unknown. An additional uncertainty lies in the demethylation connectivity between the CheB proteins and the two receptor clusters, though these questions have been the subjects of several studies, [8, 4, 6]. Although how the CheB and CheY proteins interact with the sensing and actuation modules is not known for certain, it will be shown later in the paper that under some mild assumptions, FCD can be exhibited by the bacterium regardless of the exact structure of these connectivities.

## 1.2 An MWC model of receptor dynamics

We employ an MWC-type allosteric model for the receptor activities [17]. Such models have been proposed for several bacterial chemotactic systems and have been found to be consistent with experimental data [13, 12, 7, 10]. The main assumptions of the model are that receptors are either active or inactive, and that ligands have a higher affinity for inactive receptors than for active receptors. Respectively, we denote by  $a(t)$  and  $\tilde{a}(t)$  the probabilities at time  $t$  of a transmembrane and cytoplasmic receptor being active. For each receptor, this probability can be approximated by the ratio of the Boltzmann factor of the

active state to the sum of the Boltzmann factors of all the states. Therefore if, at time  $t$ , the free-energy state of the membrane receptors is  $E_A$  when active and  $E_I$  when inactive, then the activity of the membrane receptors is approximated by

$$a(t) = \frac{\exp(-E_A)}{\exp(-E_I) + \exp(-E_A)} = \frac{1}{1 + \exp[-E_\Delta]} \quad (4)$$

where  $E_\Delta = E_I - E_A$  is the free energy difference between the active and inactive states.

Similarly for the cytoplasmic receptors, the activity  $\tilde{a}(t)$  is dependent on their free-energy states when active and inactive, respectively  $\tilde{E}_A$  and  $\tilde{E}_I$ :

$$\tilde{a}(t) = \frac{\exp(-\tilde{E}_A)}{\exp(-\tilde{E}_I) + \exp(-\tilde{E}_A)} = \frac{1}{1 + \exp[-\tilde{E}_\Delta]} \quad (5)$$

with  $\tilde{E}_\Delta = \tilde{E}_I - \tilde{E}_A$ . The functions  $E_\Delta$  and  $\tilde{E}_\Delta$  are assumed to have the same structure and take the form  $E_\Delta = -[g_m(m) + g_L(L)]$  and  $\tilde{E}_\Delta = -[\tilde{g}_m(\tilde{m}) + \tilde{g}_L(\tilde{L})]$ . The functions  $g_m, \tilde{g}_m$  are dependent on the methylation state of their respective receptors whilst the functions  $g_L, \tilde{g}_L$  quantify the effect of ligand binding on the receptor-free energy difference of the receptors. Following [10, 7, 2] we make the assumption that each of  $g_m, \tilde{g}_m$  is affinely dependent on the methylation state of its respective receptor cluster:

$$g_m(m) = \alpha(m_0 - m) \text{ and } \tilde{g}_m(\tilde{m}) = \tilde{\alpha}(\tilde{m}_0 - \tilde{m})$$

where  $\alpha = \tilde{\alpha} = 2$  and  $m_0 = \tilde{m}_0 = 5$ .

The binding of ligands to receptors leads to a loss of ligand translational entropy, proportional to the logarithm of the free ligand concentration [12, 10]. Due to the greater affinity of ligands to inactive receptors, this loss is greater in the case of ligands binding to active receptors. We denote the dissociation constants between ligands and active transmembrane (cytoplasmic) receptors by  $K_A$  ( $\tilde{K}_A$ ), and between ligands and inactive transmembrane (cytoplasmic) receptors by  $K_I$  ( $\tilde{K}_I$ ), with  $K_A \gg K_I$  and  $\tilde{K}_A \gg \tilde{K}_I$  due to the different affinities. From the *E. coli* chemotaxis literature, we adopt the values  $K_I = \tilde{K}_I = 18\mu M$ ,  $K_A = \tilde{K}_A = 3mM$ . As in [12], the change in receptor free energies due to ligand binding to active transmembrane and cytoplasmic receptors is then, respectively,  $-\ln(\frac{L}{K_A})$  and  $-\ln(\frac{\tilde{L}}{\tilde{K}_A})$ . On the other hand the change in receptor free energy due to ligand binding to inactive transmembrane and cytoplasmic receptors is, respectively,  $-\ln(\frac{L}{K_I})$  and  $-\ln(\frac{\tilde{L}}{\tilde{K}_I})$ . The effect of this on the free energy differences  $E_\Delta, \tilde{E}_\Delta$  between active and inactive receptors can be characterized, as in [12, 10], as

$$g_L(L) = \ln\left(1 + \frac{L}{K_I}\right) - \ln\left(1 + \frac{L}{K_A}\right) \text{ and } \\ \tilde{g}_L(\tilde{L}) = \ln\left(1 + \frac{\tilde{L}}{\tilde{K}_I}\right) - \ln\left(1 + \frac{\tilde{L}}{\tilde{K}_A}\right)$$

for each cluster respectively. Due to the differences in affinities, we note that  $g_L(L)$  and  $g_L(\tilde{L})$  are increasing functions of  $L$  and  $\tilde{L}$  respectively, which means that  $a(t)$  and  $\tilde{a}(t)$  are decreasing functions of  $L$  and  $\tilde{L}$  respectively. The greater affinity of ligands for inactive receptors therefore has the effect of shifting the receptors towards the inactive state.

Note that in the ligand concentration range  $K_I \ll L \ll K_A$  and  $\tilde{K}_I \ll \tilde{L} \ll \tilde{K}_A$ , the receptor activities can be approximated by

$$\begin{aligned} a &= \frac{1}{1 + \left[ \exp(\alpha[m_0 - m]) \frac{L}{K_I} \right]} \text{ and} \\ \tilde{a} &= \frac{1}{1 + \left[ \exp(\tilde{\alpha}[\tilde{m}_0 - \tilde{m}]) \frac{\tilde{L}}{\tilde{K}_I} \right]} \end{aligned} \quad (6)$$

## 2 Main results

Following similar definitions in the literature, [5, 1] we give the following definition of fold-change detection for the *R. sphaeroides* chemotaxis pathway.

**Definition 1.** *The *R. sphaeroides* chemotaxis system (1) exhibits fold change detection (FCD) in response to a sensed ligand input signal  $L(t)$  if its receptor activities  $a(t), \tilde{a}(t)$ , initially at a steady state corresponding to  $L(0)$ , are independent of linear scalings  $p > 0$  of the input  $L(t)$ .*

Note that the chemotaxis protein phosphorylation network (2) takes as its sole inputs the signals  $a$  and  $\tilde{a}$ . For this reason, Definition 1 implies that if the system (3) exhibits FCD in its activities, it also exhibits FCD in the concentration of its phosphorylated chemotaxis proteins (the elements of the vector  $\mathbf{x}$ ). The bacterium's flagellar behavior would also be expected to exhibit FCD as the flagellum rotation rate is a function of the phosphorylated CheY<sub>3</sub>, CheY<sub>4</sub> and CheY<sub>6</sub> concentrations. Before giving the main result, we make the following assumption on the chemotaxis system dynamics.

**Assumption 2.** *The system (3) has a unique steady state for any given  $L$ .*

**Theorem 1.** *Under Assumptions 1 and 2, and under approximation (6) the chemotaxis system (3), with steady state initial conditions, will exhibit FCD in its activities  $a, \tilde{a}$  for ligand inputs in the range  $K_I \ll L \ll K_A$  and  $\tilde{K}_I \ll \tilde{L} \ll \tilde{K}_A$ , in the sense of Definition 1.*

*Proof.* In the following, we assume that all ligand concentrations lie in the ranges  $K_I \ll L \ll K_A$  and  $\tilde{K}_I \ll \tilde{L} \ll \tilde{K}_A$ , and therefore approximation (6) holds. The proof is based on the existence of equivariances [1].

Suppose that in response to an external ligand input signal  $L = L_1(t)$ , the system (3), initially at a steady state corresponding to  $L = L_1(0)$ , exhibits a solution

$$\begin{bmatrix} m \\ \tilde{m} \\ \mathbf{x} \\ \xi \end{bmatrix} = \begin{bmatrix} m_1(t) \\ \tilde{m}_1(t) \\ \mathbf{x}_1(t) \\ \xi_1(t) \end{bmatrix} = \mathbf{m}_1(t)$$

and outputs  $a_1(t) = G(m_1(t), L_1(t))$ ,  $\tilde{L}_1(t) = C\xi_1 + D(u(\mathbf{x}_1, a_1))L_1^\nu$ ,  $\tilde{a}_1 = \tilde{G}(\tilde{m}_1(t), \tilde{L}_1(t))$ . Now if the ligand input is scaled to  $L = L_2(t) = pL_1(t)$ , where  $p > 0$ , and if the initial state corresponds to  $L = L_2(0)$ , then

$$\mathbf{m}_2(t) = \begin{bmatrix} m_2(t) \\ \tilde{m}_2(t) \\ \mathbf{x}_2(t) \\ \xi_2(t) \end{bmatrix} = \begin{bmatrix} m_1(t) + \frac{1}{\alpha} \log p \\ \tilde{m}_1(t) + \frac{1}{\tilde{\alpha}} \log p^\nu \\ \mathbf{x}_1(t) \\ p^\nu \xi_1(t) \end{bmatrix} \quad (7)$$

is a solution of (3) since, under approximation (6), the outputs are then

$$\begin{aligned}
a_2 &= G(m_2, L_2) \\
&= G(m_1 + \frac{1}{\alpha} \log p, pL_1) = G(m_1, L_1) = a_1 \\
\tilde{L}_2 &= C\xi_2 + D(u(\mathbf{x}_2, a_2))L_2^\nu \\
&= p^\nu C\xi_1 + D(u(\mathbf{x}_1, a_1))p^\nu L_1^\nu = p^\nu \tilde{L}_1 \\
\tilde{a}_2 &= \tilde{G}(\tilde{m}_2, \tilde{L}_2) \\
&= \tilde{G}(\tilde{m}_1 + \frac{1}{\alpha} \log p^\nu, p^\nu \tilde{L}_1) = \tilde{G}(\tilde{m}_1, \tilde{L}_1) = \tilde{a}_1
\end{aligned}$$

which means that

$$\begin{aligned}
\frac{d}{dt} \begin{bmatrix} m_2 \\ \tilde{m}_2 \\ \mathbf{x}_2 \\ \xi_2 \end{bmatrix} &= \frac{d}{dt} \begin{bmatrix} m_1(t) + \frac{1}{\alpha} \log p \\ \tilde{m}_1(t) + \frac{1}{\alpha} \log p^\nu \\ \mathbf{x}_1(t) \\ p^\nu \xi_1(t) \end{bmatrix} \\
&= \begin{bmatrix} F(a_1, w(\mathbf{x}_1)) \\ \tilde{F}(\tilde{a}_1, \tilde{w}(\mathbf{x}_1)) \\ H(\mathbf{x}_1, a_1, \tilde{a}_1) \\ p^\nu [A\xi_1 + B(u(\mathbf{x}_1, a_1))L_1^\nu] \end{bmatrix} \\
&= \begin{bmatrix} F(a_2, w(\mathbf{x}_2)) \\ \tilde{F}(\tilde{a}_2, \tilde{w}(\mathbf{x}_2)) \\ H(\mathbf{x}_2, a_2, \tilde{a}_2) \\ A\xi_2 + B(u(\mathbf{x}_2, a_2))L_2^\nu \end{bmatrix}
\end{aligned}$$

which verifies the claim that (7) is a solution of (3) when the ligand input is  $L(t) = pL_1(t)$ . Since the scaled inputs  $L = L_1(t)$  and  $L = L_2(t) = pL_1(t)$  yield the respective output pairs  $a_1, \tilde{a}_1$  and  $a_2, \tilde{a}_2$  and since  $a_1 = a_2$  and  $\tilde{a}_1 = \tilde{a}_2$ , it follows that system (3) under Assumption 1 exhibits fold change detection if the initial conditions of the system are  $\mathbf{m}_1(0)$  when  $L = L_1$  and  $\mathbf{m}_2(0)$  when  $L = L_2(t) = pL_1(t)$ . In the language of [1], we have proved that the mapping  $\mathbf{m}_1 \mapsto \mathbf{m}_2$  is an equivariance associated to scalar symmetries on inputs.

Now if the system has a unique fixed point for any given  $L$ , and if  $\mathbf{m}_1(0)$  is the fixed point when  $L = L_1(0)$ , then  $\mathbf{m}_2(0)$  is the fixed point when  $L = L_2(0) = pL_1(0)$  since, if  $\dot{\mathbf{m}}_1 = \mathbf{0}$  when  $L = L_1(0)$  then  $\dot{\mathbf{m}}_2 = \mathbf{0}$  when  $L = L_2(0) = pL_1(0)$ . Therefore if system (3) has a unique fixed point for any given  $L$ , starts from steady state conditions and yields solution  $\mathbf{m}_1(t)$ , then scaling  $L$  by  $p > 0$  and initiating the system from steady state conditions will cause the system to yield the solution  $\mathbf{m}_2(t)$  and thereby exhibit FCD.  $\square$

### 3 Two *R. sphaeroides* chemotaxis models

There are several integrated *R. sphaeroides* chemotaxis pathway models in the literature [4, 8, 6]. In this section, we present two new models, differing from the previous ones in that their receptor dynamics are of the form (3) and satisfy the MWC model given in Section 1.2. Both of the new models we present were fitted to experimental data available in [4] and were able to reproduce the gene deletion data in [8, 4].

Each of the models presented satisfies the assumptions of Section 1.2 and thereby exhibits FCD in the ligand range  $K_I \ll L \ll K_A$  and  $\tilde{K}_I \ll \tilde{L} \ll \tilde{K}_A$ . The demethylating feedback



structure for the models is restricted to that in [4], which proposed an asymmetric feedback structure wherein CheB<sub>1</sub> demethylates both clusters and CheB<sub>2</sub> demethylates the cytoplasmic cluster, although a model with any feedback connectivity is capable of exhibiting FCD under the assumptions we make.

The structural differences between the models lie in the signal  $\tilde{L}$ , which captures how external ligands are transduced to the cytoplasmic cluster. These models illustrate the point that, despite the differences in their internal connectivities, FCD behavior is conserved under the assumptions above.

Following [16, 4], we make the assumptions that CheB proteins demethylate active receptors, whilst CheR proteins methylate inactive receptors, and that CheR proteins operate at saturation. The CheR<sub>2</sub> and CheR<sub>3</sub> protein concentrations are therefore assumed to be constant and normalized to  $1\mu M$  each. Denoting by  $R_2, R_3$  the concentrations of CheR<sub>2</sub> and CheR<sub>3</sub> and by  $B_{1_p}, B_{2_p}$  the concentrations of phosphorylated chemotaxis proteins CheB<sub>1</sub>, CheB<sub>2</sub>, mass action kinetics give the following general form for  $F, \tilde{F}$  in (3)

$$\begin{aligned}\dot{m} &= F(a, \tilde{a}, w(\mathbf{x})) = k_R(1 - a)R_2 - k_{B_1}B_{1_p}a - k_{B_2}B_{2_p}a \\ \dot{\tilde{m}} &= \tilde{F}(a, \tilde{a}, \tilde{w}(\mathbf{x})) = \tilde{k}_R(1 - \tilde{a})R_3 - \tilde{k}_{B_2}B_{2_p}\tilde{a}\end{aligned}\quad (8)$$

where  $k_R, \tilde{k}_R > 0$  are methylation and  $k_{B_1}, k_{B_2}, \tilde{k}_{B_2} > 0$  demethylation rate constants. The probabilities of activity  $a, \tilde{a}$  given by (4), (5). The models were obtained by fitting the constants  $k_R, \tilde{k}_R, k_{B_1}, k_{B_2}, \tilde{k}_{B_2}$  in (8).

The experimentally measured output which was used to fit the model is the flagellar rotation frequency  $f$ . As shown in Figure 2, the CheY proteins control the rotation of the flagellum, and this is believed to happen through inhibitory binding [8]. The measured rotation frequencies to which we fit our models varied between 0 Hz and a maximum of approximately 8 Hz. As discussed in [4], this maximum was very rarely exceeded, and is therefore assumed to be a physical limit on how fast the flagellum can rotate. As such, the rotation frequency is modeled as the Hill function

$$f = -\frac{1}{0.125 + \phi(Y_{3_p}, Y_{4_p}, Y_{6_p})^4}$$

where

$$\phi(Y_{3_p}, Y_{4_p}, Y_{6_p}) = 0.012Y_{6_p} \frac{Y_{3_p} + Y_{4_p}}{0.1 + Y_{3_p} + Y_{4_p}}$$

(the negative sign denotes anti-clockwise rotation). In this way,  $f$  varies between 0 - 8 Hz, and decreases with increased concentrations of phosphorylated CheY proteins.

### 3.0.1 Model I

**Model structure:** In this model the cytoplasmic receptors are assumed to sense internalized ligands, the concentrations of which are dependent on the external ligand concentration  $L$ . At the same time, as in [4], we assume there to be some interaction between the chemotaxis proteins CheY<sub>3</sub>, CheY<sub>4</sub> and the cytoplasmic cluster, and the function  $\tilde{g}_L(\tilde{L})$  takes as its input  $\tilde{L} = \frac{10L}{10 + Y_{3_p} + Y_{4_p}}$ . A schematic of this model is shown in Figure 4.

A simulation of the model together with the tethered cell trace to which the model was fitted is shown in Figure 5. For comparison, Figure 5 additionally shows a simulation (with the same ligand input) of the model suggested in [4], which was fitted to the same tethered cell assay. The root mean squared error between the output of Model I and the tethered

cell assay is 0.88, which compares favorably to the corresponding error for the model in [4], which is 1.27.

This model would be expected to exhibit FCD in the ligand ranges  $K_I \ll L \ll K_A$  and  $\tilde{K}_I \ll \tilde{L} \ll \tilde{K}_A$ . The latter range is equivalent to

$$\tilde{K}_I (1 + 0.1[Y_{3_p} + Y_{4_p}]) \ll L \ll \tilde{K}_A (1 + 0.1[Y_{3_p} + Y_{4_p}])$$

and since the total amounts of intracellular CheY<sub>3</sub> and CheY<sub>4</sub> (phosphorylated and unphosphorylated) are 3.2μM and 13.2μM respectively, then according to this model, simulations should show FCD in the range  $2.64\tilde{K}_I \ll L \ll \tilde{K}_A$ . Figure 6 shows that this is indeed the case, with similar output traces obtained for the step changes in  $L$  from  $L = 1000\mu\text{M}$  to  $200\mu\text{M}$  and from  $L = 500\mu\text{M}$  to  $100\mu\text{M}$ .

**Model parameters:**  $k_R = \tilde{k}_R = 0.0045$   $k_{B_1} = \tilde{k}_{B_2} = 2.116$   $k_{B_2} = 2.822$ .

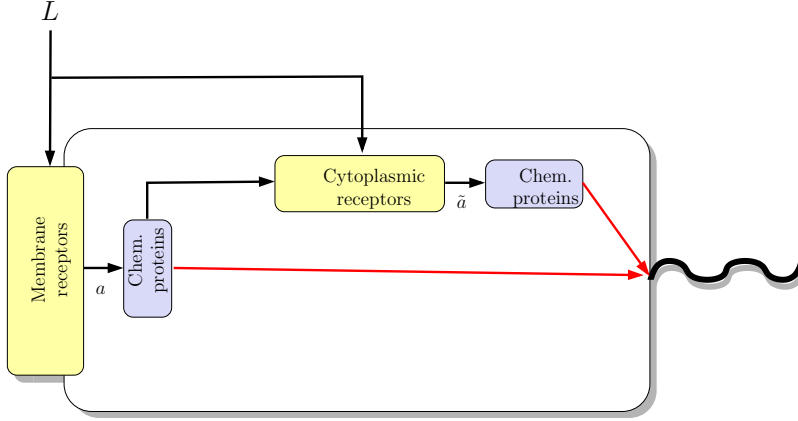


Figure 4: Schematic of Model I.

### 3.0.2 Model II

**Model structure:** Here, the model's internally sensed ligands  $\tilde{L}$  are related to  $L$  via the differential equation  $\dot{\tilde{L}} = -\frac{1}{2}\tilde{L} + \frac{1}{2}L$ . Whilst the ligand concentrations  $L, \tilde{L}$  modify receptor activities, the cytoplasmic receptors are otherwise unregulated by internal cell signals, and therefore  $\tilde{L}$  is not a function of  $u$ . A schematic is illustrated in Figure 7, and a simulation of the model together with the tethered cell trace to which the model was fitted is shown in Figure 8. For comparison, Figure 8 additionally shows a simulation (with the same ligand input) of the model suggested in [4], which was fitted to the same tethered cell assay. The root mean squared error between the output of Model II and the tethered cell assay is 0.95, which, as with Model I, also compares favorably to the corresponding error for the model in [4], which is 1.27.

Note that if  $L$  were to undergo a step change from  $L = L_a\mu\text{M}$  to  $L = L_b\mu\text{M}$  and if the system is initially at steady state (where  $\tilde{L}(0) = L_a$ ), then  $\tilde{L}$  would remain confined to the set  $[L_a, L_b]$ . Therefore, for such a step change,  $K_I \ll L \ll K_A$  implies that  $\tilde{K}_I \ll \tilde{L} \ll \tilde{K}_A$ . Figure 9 shows that simulations of this model do show FCD in this input range, with similar

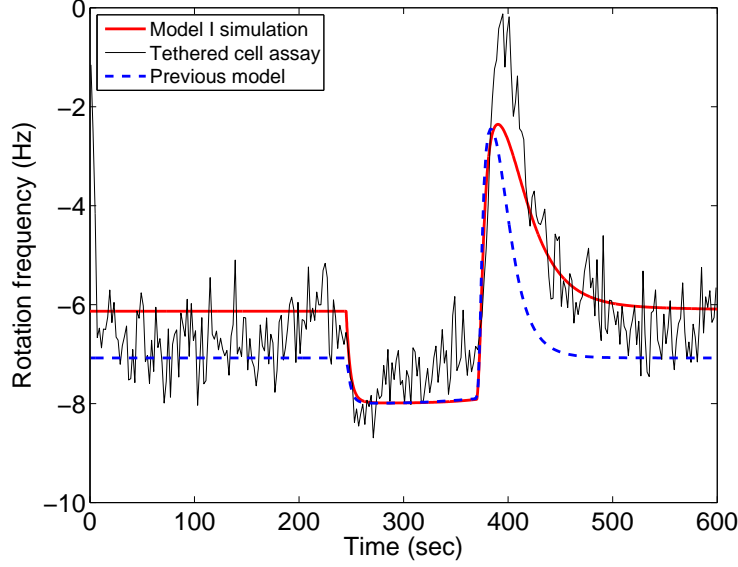


Figure 5: Simulation of Model I (red) in response to a step rise (at 245 seconds) and fall (at 370 seconds) in the ligand level  $L$  from  $L = 0$  to  $L = 100$  and back to  $L = 0$ , with a tethered cell assay (black). The dashed blue trace is a simulation of the previously published model in [4] subject to the same ligand input.

output traces obtained for the step changes in  $L$  from  $L = 1000\mu\text{M}$  to  $200\mu\text{M}$  and from  $L = 500\mu\text{M}$  to  $100\mu\text{M}$ .

**Model parameters:**  $k_R = \tilde{k}_R = 0.0057$   $k_{B_1} = \tilde{k}_{B_2} = 2.376$   $k_{B_2} = 2.970$ .

### 3.1 Future experiments for model invalidation

The models presented above are two systems based on the assumptions of Section 1.2 that reproduce the experimental data of [4], but which additionally show FCD. By comparison, the model suggested in [4], based on different receptor dynamics, does not exhibit FCD in response to the inputs used in the simulation in Figures 6, 9 as shown in Figure 10.

One important feature to note is that the FCD property is preserved regardless of the exact dynamics in (2) and regardless of the interactions between the receptors and the chemotaxis proteins, as long as the conditions of Theorem 1 are satisfied. Therefore, if the receptor dynamics model given in Section 1.2 is accurate, then in the ligand concentration ranges  $K_I \ll L \ll K_A$  and  $\tilde{K}_I \ll \tilde{L} \ll \tilde{K}_A$ , FCD is a robust dynamic property of the chemotaxis system that should be observed in both wild type and in mutant strains of *R. sphaeroides* that have chemotaxis protein deletions and over-expressions.

The above points suggest experiments in which the FCD dynamic phenotype can be used to discriminate between Models I and II on the one hand, and the model suggested in [4] on the other:

- If Models I and II are to invalidate that of [4] then the wild type bacterium, initially at steady state, should show near identical flagellar output responses to the step ligand

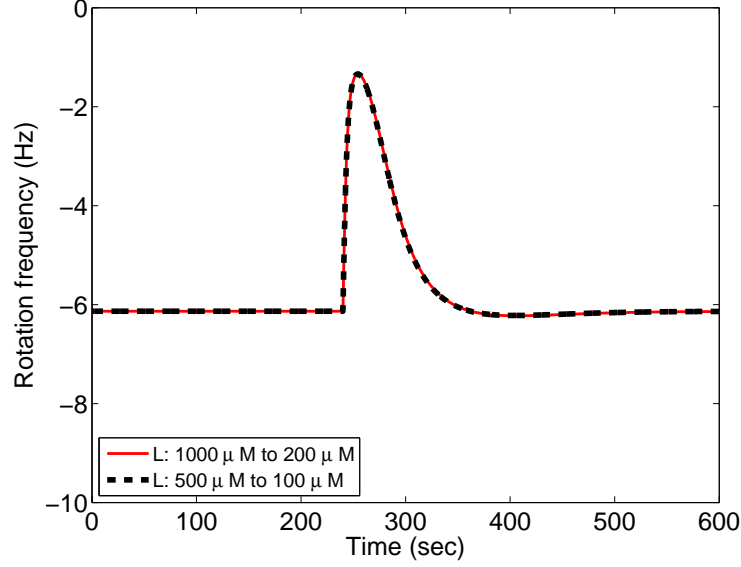


Figure 6: Model I output in response to step changes in  $L$  from  $L = 1000\mu\text{M}$  to  $200\mu\text{M}$  and from  $L = 500\mu\text{M}$  to  $100\mu\text{M}$

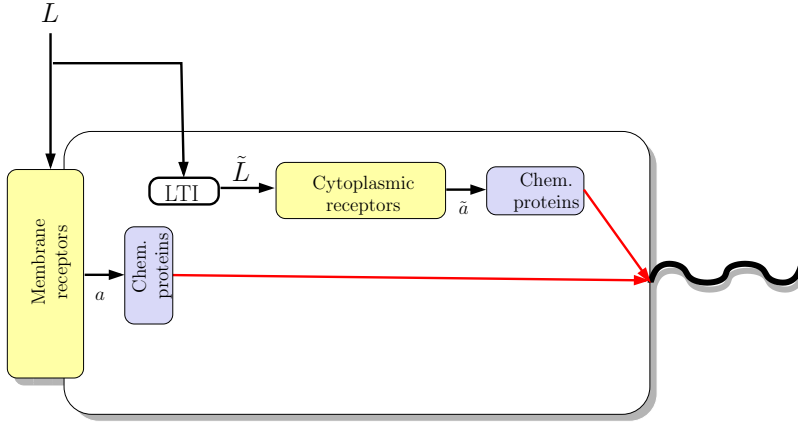


Figure 7: Schematic of Model II.

inputs  $L = 1000\mu\text{M}$  to  $200\mu\text{M}$  and  $L = 500\mu\text{M}$  to  $100$ .

- Overexpressing the chemotaxis protein CheY<sub>4</sub> five fold was shown in [8] to not destroy the chemotactic response of the bacterium. Such a mutant strain should therefore, according to Models I and II, also exhibit FCD in response to a range of step changes in the external ligand concentration  $L$ . We can calculate this range for each of the two models as in Sections 3.0.1 and 3.0.2. In Model I, the five-fold increase in CheY<sub>4</sub> means that FCD should be observed within the range  $7.92\tilde{K}_I \ll L \ll \tilde{K}_A$ , whereas

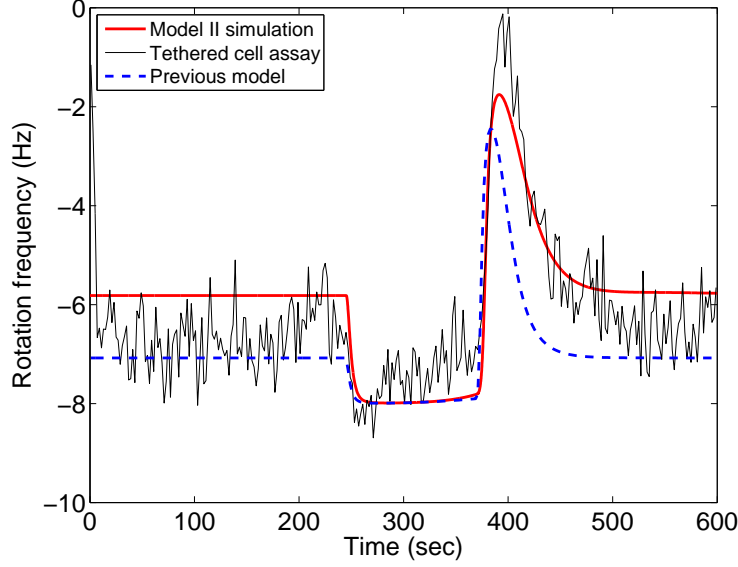


Figure 8: Simulation of Model II (red) in response to a step rise (at 245 seconds) and fall (at 370 seconds) in the ligand level  $L$  from  $L = 0$  to  $L = 100$  and back to  $L = 0$ , with a tethered cell assay (black). The dashed blue trace is a simulation of the previously published model in [4] subject to the same ligand input.

for Model II this range is  $\tilde{K}_I \ll L \ll \tilde{K}_A$ .

- If we define the adaptation time when the model is subject to a step decrease in ligand to be the time that it takes from the application of the step for the deviation of the flagellar rotation frequency from its steady-state value to fall to 25% of its maximum, then under this definition, the adaptation times for Models I and II are 65 seconds and 62 seconds respectively, whereas for the model in [4], the adaptation times are 266 seconds for the step ligand concentration decrease of  $1000 \mu\text{M}$  to  $200 \mu\text{M}$ , and 162 seconds for the step decrease of  $500 \mu\text{M}$  to  $100 \mu\text{M}$ . If Models I and II are to invalidate those in [4], the experiments should yield approximately equal adaptation times in response to these two step changes in ligand concentration, and these adaptation times should be around 60 seconds.

Further model discrimination between Models I and II can be performed using the tools presented in [8, 4].

## 4 Discussion

The models presented herein differ from earlier *R. sphaeroides* chemotaxis models in two main respects: first, the receptor dynamics are based on the MWC allosteric model. This model has been shown to be a fairly accurate representation of the receptor dynamics in *E. coli*. The homologies between the bacteria and the similarities between their overall chemotaxis mechanisms give us reason to believe that the MWC model may, under experimental

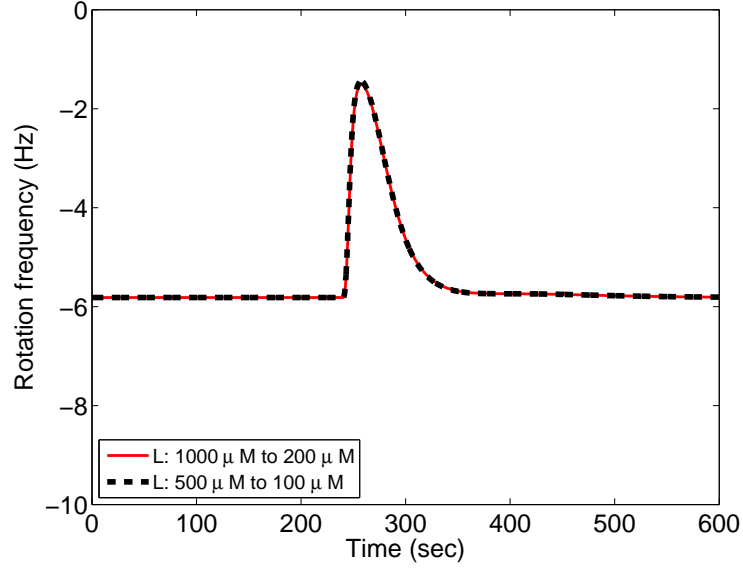


Figure 9: Model II output in response to step changes in  $L$  from  $L = 1000\mu\text{M}$  to  $200\mu\text{M}$  and from  $L = 500\mu\text{M}$  to  $100\mu\text{M}$

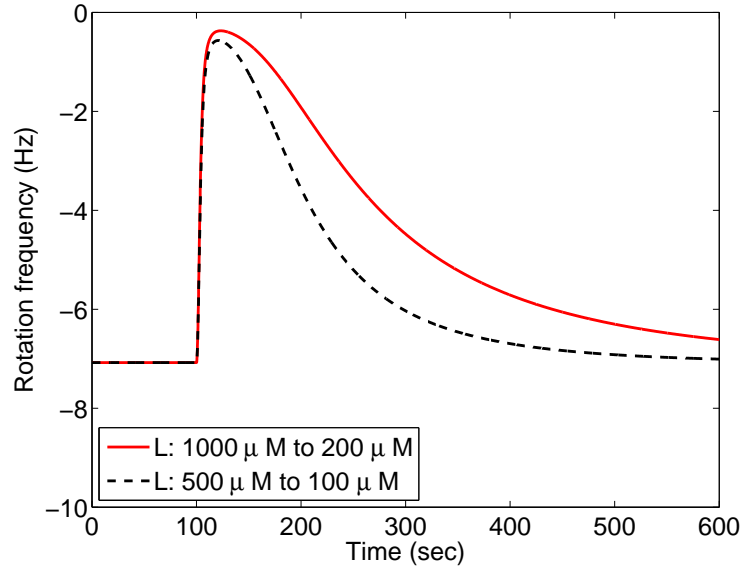


Figure 10: Simulations of the model in [4], subject to step changes in  $L$  from  $L = 1000\mu\text{M}$  to  $200\mu\text{M}$  and from  $L = 500\mu\text{M}$  to  $100\mu\text{M}$

testing, eventually prove to be a realistic way of representing the *R. sphaeroides* receptor

dynamics.

The second point of departure of these models from earlier ones is that the assumptions on the possible relationships between the external and internal ligand concentrations are relaxed to admit dynamic relations. The motivation behind this model is to capture any phase delays between sensed changes in the external ligand concentration and the effect of such changes on the internal cell environment.

The external-internal ligand relation of Model I closely follows that of [4]. In effect, the activity of the cytoplasmic cluster depends on the external ligand concentration,  $L$ , and, indirectly, on the activity  $a$  of the membrane cluster via the phosphorylated chemotaxis proteins CheY<sub>3</sub>-P and CheY<sub>4</sub>-P, as schematically illustrated in Figure 4. On the other hand, the cytoplasmic receptor activity in Model II does not depend on any chemotaxis proteins, and its sensed ligand signals are merely phase-delayed versions of the external ligand concentration.

As experimentally shown [3], chemotaxis requires CheY<sub>6</sub> *and* one of either CheY<sub>3</sub> or CheY<sub>4</sub>, as deletion of either CheY<sub>6</sub> or both of CheY<sub>3</sub><sub>p</sub> and CheY<sub>4</sub><sub>p</sub> destroys the chemotactic ability of the bacterium. In the models we present, this was captured by the interaction of the three CheY proteins at the flagellum in what is effectively an AND logic gate that will only be activated if both CheY<sub>6</sub> and at least one of CheY<sub>3</sub><sub>p</sub> or CheY<sub>4</sub><sub>p</sub> are present. The signal transduction dynamics ([14, 8]) show that CheY<sub>3</sub><sub>p</sub> and CheY<sub>4</sub><sub>p</sub> are solely phosphorylated by the membrane cluster, whereas CheY<sub>6</sub> receives most of its phosphates from the cytoplasmic cluster. In essence, this structure means that there are essentially two paths from the external ligands to the flagellum that terminate at the AND gate: one path via the membrane cluster in which CheY<sub>3</sub><sub>p</sub> and CheY<sub>4</sub><sub>p</sub> proteins convey the signal, and one path via the cytoplasmic cluster, in which CheY<sub>6</sub><sub>p</sub> conveys the signal. This resembles a recurring biochemical motif [11], and the selective advantage it bestows could be improved *energy taxis* [3] with respect to simpler chemotaxis circuits such as that of *E. coli*. The main feature of this improved pathway is that the flagellar motion will only vary if both signalling paths from  $L$  to the flagellum are activated. Since the cytoplasmic cluster may integrate un-modeled metabolic information from within the cell, it would be important that any variation in flagellar activity only results from a change in the metabolic state of the cell that arises from a change in the local chemoeffector environment. If this is indeed the case then the signalling path from the cytoplasmic cluster is only activated if the metabolic state of the cell changes, whilst the signalling path from the membrane cluster is only activated if the immediate chemical environment changes. Only if both are activated together would the cell ‘know’ that the change in its metabolic state is due to a change in chemoeffector concentration, and only then would it change its flagellar activity.

#### 4.1 Selective advantage of FCD

Whether FCD bestows upon the bacterium a selective advantage or simply arises as a by-product of the chemotaxis system’s structure is a question of interest. The fact that FCD is present in simpler chemotaxis circuits than that of *R. sphaeroides* (e.g. in *E. coli*) suggests that the advantages gained by having such a property would be independent of the complexity of the bacterium’s chemotaxis pathway. It may be that the metabolic payoff to the bacterium of moving to more chemically favorable regions depends on the relative chemical improvement in its environment rather than the absolute change. A reason for this could be that biasing its movement towards longer swims could be metabolically costly for the bacterium, and moving in this way is only worthwhile if the metabolic gain is

significant. A potential disadvantage of FCD to the bacterium could be a high sensitivity to small fluctuations in sensed ligand when the background ligand concentration is low, due to the fact that the gain in the flagellar rotation frequency would then be high. However, this disadvantage is offset by the fact that FCD behavior only occurs at background ligand concentrations significantly above a threshold, given by  $K_I$  in the models above.

## 4.2 FCD as dynamic phenotype for model invalidation

The models we have presented provide an example of how dynamic phenotypes can be used to discriminate between competing biochemical models. Given two models of the same system, a mathematical analysis can be used to identify regions in the parameter and input spaces in which a certain qualitative dynamic behavior, such as FCD, could be expected. Ideally, this behavior would be expected to be robust to any genetic mutations or environmental conditions, and the conditions under which this behavior would occur would be implementable experimentally. Model discrimination can then be performed on the basis of whether or not the system robustly reproduces the dynamic phenotype experimentally. This differs from traditional forms of model discrimination in that it can be used to discriminate between different biological mechanisms, and can be used to identify whether an observed phenomenon is due to the fine tuning of biological parameters or due to a more fundamental structural property of the system.

## References

- [1] Shoval O, Alon U, and Sontag ED (2011). *Symmetry invariance for adapting biological systems*. SIAM J Appl Dyn Syst, 10:857-886.
- [2] Lazova MD, Ahmed T, Bellomo D, Stocker R, Shimizu TS (2011). *Response rescaling in bacterial chemotaxis*. Proc Natl Acad Sci USA 108(33): 1387013875.
- [3] Porter SL, Wadhams GH, Armitage JP (2011) *Signal processing in complex chemotaxis pathways*. Nat Rev Microbiol 9(3):153-65.
- [4] Hamadeh A, Roberts M, August E, McSharry P, Maini P, Armitage J, Papachristodoulou A (2011). *Feedback control architecture and the bacterial chemotaxis network*. PLoS Comp Biol 7(5):e1001130.
- [5] Shoval O, Goentoro L, Hart Y, Mayo A, Sontag E, and Alon U (2010). *Fold-change detection and scalar symmetry of sensory input fields*. Proc Natl Acad Sci USA 107(36):1599516000.
- [6] Tindall MJ, Porter SL, Maini PK, Armitage JP (2010). *Modeling Chemotaxis Reveals the Role of Reversed Phosphotransfer and a Bi-Functional Kinase-Phosphatase*. PLoS Comp Biol 6(8):e1000896.
- [7] Clausznitzer D, Oleksiuk O, Lvdok L, Sourjik V, Endres RG (2010). *Chemotactic Response and Adaptation Dynamics in Escherichia coli*. PLoS Comp Biol 6(5):e1000784.
- [8] Roberts M, August E, Hamadeh A, Maini P, McSharry P, Armitage J, Papachristodoulou A (2009). *A new approach for elucidating biological signalling networks*. BMC Syst Biol, 3:105.



- [9] Pilizota T, Brown MT, Leake MC, Branch RW , Berry RM, Armitage JP (2009) *A molecular brake, not a clutch, stops the Rhodobacter sphaeroides flagellar motor*. Proc Natl Acad Sci USA 106(28):11582-11587.
- [10] Tu Y, Shimizu TS, Berg HC (2008). *Modeling the chemotactic response of Escherichia coli to time-varying stimuli*. Proc Natl Acad Sci USA 105(39):14855-14860.
- [11] Alon, U (2006). *An Introduction to Systems Biology: Design Principles of Biological Circuits*. Chapman & Hall/CRC Mathematical & Computational Biology.
- [12] Keymer JE, Endres RG, Skoge M, Meir Y, Wingreen NS (2006). *Chemosensing in Escherichia coli: Two regimes of two-state receptors*. Proc Natl Acad Sci USA 103(6):1786-1791.
- [13] Sourjik V, Berg HC (2004). *Functional interactions between receptors in bacterial chemotaxis*. Nature 428: 437-441.
- [14] Porter SL, Armitage JP (2002) *Phosphotransfer in Rhodobacter sphaeroides chemotaxis*. J Mol Biol 324: 35-45.
- [15] Yi TM, Huang Y, Simon MI, Doyle J (2000). *Robust perfect adaptation in bacterial chemotaxis through integral feedback control*. Proc Natl Acad Sci USA 97(9):4649-4653.
- [16] Barkai N, Leibler S (1997). *Robustness in simple biochemical networks*. Nature 387:913-917.
- [17] Monod J, Wyman J, Changeux JP (1965). *On the nature of allosteric transitions: A plausible model*. J Mol Biol 12: 88-118.